A Stress Intensity Function for FCG Analyses in Metals

Daniel Kujawski
Mechanical and Aerospace Engineering,
Western Michigan University, Kalamazoo, MI, 49008, USA

Abstract

This paper presents a damaging stress intensity function K_d for analyses of R-ratio effects on fatigue crack growth (FCG) in metals. The proposed formulation is based on the sum of strain and complementary energy and its role in FCG rate behavior in threshold and Paris region at R-ratios ranging from -2 to 0.97. It doesn't invoke a crack closure assumption or fitting parameters for R<0.5-0.6. For a high R>0.7 it utilizes an experimentally determine correction factor, which accounts for excessive plastic dissipation in the monotonic plastic zone (MPZ).

Key words: *R-ratio effects; Constant amplitude FCG analyses; Two-parameter driving force K_{max} and K_a; FCG of steel, Al, Ti, and copper alloys.*

1.0 Introduction

Understanding and modeling of fatigue crack growth (FCG) rate and its dependence on R-ratio (R=minimum load/maximum load) is a prerequisite for safe life predictions of components in service. In 1960's Paris and Erdogan [1] proposed to corelate FCG rate, (da/dN), in terms of an applied stress intensity factor (SIF) range ΔK in the form of

$$\frac{da}{dN}=C(\Delta K)^m \tag{1}$$

where C and m are fitting parameters.

In such analysis, each R-ratio forms a discreet (da/dN) vs. ΔK curve. In 1970 Elber [2] proposed to account for R-ratio effects by substituting in Eq. (1) for ΔK an effective SIF range ΔK_{eff} defined as:

$$\Delta K_{eff} = K_{max} - K_{OP} \text{ (or } K_{CL}) \tag{2}$$

where K_{OP} is the SIF corresponding to crack opening when there is no contact in the crack wake during loading. Commonly, K_{OP} term is used interchangeably with K_{CL} where K_{CL} correspond to crack closure during unloading. Elber has observed experimentally, that the crack flanks come to premature contacts and explained his observation based on a concept of plasticity induced

crack closure (PICC). Then he suggested that only the sole driving force ΔK_{eff} is sufficient to collapse all different R-ratio da/dN data into a single curve in the form of:

$$\frac{da}{dN} = C^{¿} \left(\Delta K_{eff} \right)^{m^{¿}} \tag{3}$$

where C^* and m^* are fitting parameters and usually $m^{¿} \cong m$.

An empirical Eq. (3) requires generating experimentally or numerically a closure free da/dN-ΔK_{eff} master curve and it becomes an accepted method for FCG analysis, for the last 50 years.

From the experimental viewpoint, at the near-threshold region, difficulties occur in the determination of Eq. (2) due to low resolution in the load-displacement slopes used for measuring K_{OP} (or K_{CL}) level. It has been pointed out [3-7] that K_{OP} (or K_{CL}) measurements are difficult at near threshold region. In the past several decades, three major experimental methods have been developed to establish K_{OP}. To date, these methods are [8]: (1) Compliance techniques using a load-displacement curve that utilize strain or displacement gauges located in a far-field or near crack-tip locations, (2) Crack propagation techniques, (3) Non-mechanical contact measurements using digital imaging. Among these methods, it is claimed that near crack-tip gauges are more sensitive to measure load displacement trace in comparison to the far-field ones. Detailed discussion on these techniques their limitations and advantages can be found in recent comprehensive review by Pippan and Hohenwater [8].

There is a common agreement among researchers, who use ΔK_{eff} approach, at R ¿ 0.6-0.7 as a closure free region, yet R-ratio effects are still observed, in particular near the threshold region. Using a better resolution measurement set up, Newman and co-workers [9] detected a slope change in the load versus reduced strain curve for tests at R = 0.9. This deviation was also attributed to crack closure. However, this isolated observation has not been reproduced by other investigators. To date, crack closure concepts have not yet been able to consistently describe the near-threshold FCG behavior in many alloys [8].

Another approach accounting for R-ratio effects on FCG without crack closure assumption was proposed by Walker in 1970 [10].

$$\Delta K_W = K_{max}^{(1-\gamma)} \Delta K^{\gamma} \tag{4}$$

where γ is the fitting parameter and ΔK_W is the equivalent SIF corresponding to R = 0 where $\Delta K=K_{max}$. Experimental results indicate that Eq. (4) correlates the data only for positive R-ratios [11]. Hence, several attempts have been proposed in the literature to modified Walker parameter [12,13]. However, due to a lack of sound physical foundation, Walker Eq. (4) and its modifications were not so widely used as the crack closure approach.

On the other hand, about 25 years ago, Sadananda and Vasudevan [14, 15] postulated that Eq. (1) is valid only for R=0 where both ΔK and K_{max} are equal. They advocated, that FCG is a two-parameter damaging process controlled by ΔK and K_{max}. Hence, at threshold both thresholds ΔK_{th} and $K_{max,th}$ must be satisfied simultaneously for a crack to propagate. If only one of them is satisfied the crack would arrest and not propagate. Thus, for crack extension to occur, the applied $\Delta K > \Delta K_{th}$ and applied $K_{max} > K_{max,th}$. This two-parameter dependence results in a L-shape curve for a given da/dN =constant in terms of K_{max} and ΔK signifying that they are interrelated [14,15]. On the other hand, Chandran [16.17] demonstrated that FCG behavior and its dependence on R-ratio can be correlated by utilizing the net section energy release rate.

Recently, Tong et al. [18] in 2019 and Gonzales et al. [19] in 2020 demonstrated that crack closure, although identifiable in the compliance curves or by imagine correlation technique does not appear to impact on the global crack driving force. Tong et al. concluded that the ΔK_{eff} is a misconception whereas Gonzales et al. stated that the ΔK_{eff} is not a useful FCG driving force for FCG analysis. Very recently we showed that threshold $K_{max,th}$ is related to K_{OP} through a critical monotonic plastic strain [20]. This trend in K_{OP} vs $K_{max,th}$ seems to be a general behavior for many different structural materials, under different environments, and load ratios [20]. Despite reported experimental challenges and limitations associated with crack closure, so far, the ΔK_{eff} approach has been dominated.

The present article proposes a new damaging SIF function for analysis and modeling of FCG including R-ratio effects. This damaging SIF function, which drive the fatigue crack comprises the strain and complementary energy densities and accounts also for dissipative processes associated with plasticity in a monotonic plastic zone. Instead of conventional ΔK_{eff}

given by Eq. (2), we proposed a damaging SIF function K_d to model and analyze R-ratio effects on da/dN behavior.

2.0 Background

This section discusses similarities and differences between cracked and smooth specimens subjected to cyclic loading and associated parallels and links.

Let us consider, smooth versus cracked specimens which are subjected to a constant amplitude cyclic loading with the remotely applied load varied between P_{min} and P_{max} such as $P_{min}/P_{max} > 0$. In the case of the smooth specimen, the distribution of stress σ and strain ε is homogenous and the applied load ratio, $R = P_{min}/P_{max} = \sigma_{min}/\sigma_{max}$. In contrast, the distribution of the stress and strain in the crack tip region of the cracked specimen is highly inhomogeneous, and in this case $R = P_{min}/P_{max} \neq \sigma_{min}/\sigma_{max}$. Figure 1a shows schematically the local maximum stress distribution σ_{max} as a full line and the local minimum stress distribution σ_{min} by a dashed line for loading at R > 0. The local cyclic stress history ahead of the crack tip along the x-axis, is depicted in Fig. 1a by the zig-zag curves together with the monotonic (MPZ) and cyclic (CPZ) plastic zones.

A schematic distribution of the local stress ratio R_σ along the crack path is shown in Fig. 1b. It is seen from Fig. 1b that for $x > r_{MPZ}$ the local stress ratio R_σ tends to approach to the applied R. Within the MPZ where $r_{CPZ} < x < r_{MPZ}$ the R_σ decreases (in algebraic sense) as the material point moves towards the crack tip and accumulates the monotonic plastic strain. In this region a steep gradient of the local stress ratio R_σ is expected, which is dependent upon ΔK and R. For the material element at $x \leq r_{CPZ}$, and assuming the kinematic hardening rule, the local stress ratio R_σ, can be estimated as.

$$R_\sigma = \sigma_{min}/\sigma_{max} = \left(\sigma_{max} - 2\sigma_0\right)/\sigma_{max} = 1 - 2\left(\sigma_0/\sigma_{max}\right) \qquad (5)$$

It has been widely recognized that a small zone, termed here in as a 'process zone" , d^*, exist immediately ahead of the crack tip where due to crack tip blunting , the stress and strain have finite magnitude with a small gradient. Therefore, as an approximation, for a material element within the process zone d^* a constant value of $R_\sigma \cong$ -1 can be assumed. For example, in the case

of an elastic-perfectly plastic material, $\sigma_{max}=\sigma_0$ for $x \le r_{CPZ}$ which implies a constant R_σ = -1 within the CPZ. Consequently, for low strain hardening materials, the cyclic stresses, and strains within the process zone resemble approximately a uniaxial loading of smooth specimen at R ≅ -1, as it is illustrated in Fig. 1c. Hence, the fatigue damage within the process zone, d^*, can be approximated to that experiences by the smooth specimen where $R \approx -1$.

Using the analogy between a smooth specimen cycling at $R=-1$ and the material within the process zone with local $R_\sigma \approx -1$ we will adopt recently proposed modified SWT function [21] in terms of the total damaging energy density W_d. The total damaging energy density, W_d, for fully reversed loading is given by Eq. (6):

$$W_d = W_S + W_C \; when \; both \; \sigma_d \ge 0 \wedge \varepsilon_d \ge 0 \qquad (6)$$

W_d is the sum of the strain energy density W_S and complementary energy density W_C, which are calculated at the first quadrant in damaging σ_d-ε_d axes, as it is depicted in Fig. 2a. For fully reversed loading with σ_m = 0, the damaging and stress-strain axes associated with a stabilized hysteresis loop overlap, i.e. $\sigma_d = \sigma$ and $\varepsilon_d = \varepsilon$. For the stabilized hysteresis loop with $\sigma_m \ge 0$, dislocations move back and forth around $\pm\varepsilon_m$. Therefore, for $\sigma_m \ge 0$ damaging σ_d axis would pass through ε_m, whereas the $\varepsilon_d = \varepsilon$ as it shown in Fig. 2b. Hence, the total damaging energy density W_d is equivalent to the *SWT* function] and is calculated as:

$$W_d = \sigma_{max}\varepsilon_a \; valid \; for \; \sigma_m \ge 0 \qquad (7a)$$

For cyclic loading with negative mean stress ($\sigma_m < 0$) the maximum stress is augmented by the positive part of deviatoric component of the mean stress as it is shown in Fig. 2c and the corresponding W_d is calculated as.

$$W_d = (\sigma¿¿max + |\sigma_m|/3)\varepsilon_a \; valid \; for \; \sigma_m < 0¿ \qquad (7b)$$

Equation (7b) is called the modified $mSWT$ function.

In terms of the stress formulation Eq. (7) would take the following forms:

$$\sigma_{ar} = \sqrt{\sigma_{max}\sigma_a} \quad \textit{valid for } \sigma_m \geq 0 \tag{8a}$$

and

$$\sigma_{ar} = \sqrt{(\sigma¿¿max + |\sigma_m|/3)\sigma_a¿} \quad \textit{valid for } \sigma_m < 0 \tag{8b}$$

where σ_{ar} is an equivalent fully reversed stress amplitude.

Both Eqs. (7) and (8) shows a consistent correlation of the mean stress effects for both positive and negative mean stresses. The stress-based function given by Eq. (8) is adopted in this paper in terms of the SIF values as it is discussed in detail in Section 4.

3.0. Analyses of Monotonic and Cyclic Plastic Zones at SSY

Mode I of FCG under small scale yielding (SSY) condition is associated with a complex elastic-plastic deformation along the path of crack propagation as illustrated in Fig. 1. At a location far away from the crack tip the material experiences only elastic strains. As a crack tip moves towards the material reference point, at some distance, it enters the monotonic plastic zone (MPZ) and subsequently, as the crack propagates further, the material reference point enters a cyclic plastic zone (CPZ), which is embedded within the MPZ.

For a plane stress condition, the size of the MPZ_σ can be estimated as:

$$MPZ_\sigma = \frac{1}{\pi}\left(\frac{K_{max}}{\sigma_0}\right)^2 \tag{9}$$

and for a plane strain condition as:

$$MPZ_\varepsilon = \frac{1}{3\pi}\left(\frac{K_{max}}{\sigma_0}\right)^2 \tag{10}$$

where σ_0 is the 0.2% offset yield strength.

The ratio of the MPZ at a given R-ratio, MPZ_R, over the corresponding MPZ_0 at R=0, for both plane stress and plane strain, can be estimated from Eq. (9) or (10) as:

$$\frac{MPZ_R}{MPZ_0}=\left(\frac{K_{max,R}}{K_{max,0}}\right)^2 \tag{11}$$

where $K_{max,R}$ and $K_{max,0}$ are the corresponding maximum values of SIF at a given R and R=0, respectively.

Assuming a kinematic hardening where the range of elastic domain is $2\sigma_0$, the CPZ can be estimated for a plane stress as:

$$CPZ_\sigma=\frac{1}{2\pi}\left(\frac{\Delta K}{\sigma_0}\right)^2 \tag{12}$$

and for a plane strain:

$$CPZ_\varepsilon=\frac{1}{6\pi}\left(\frac{\Delta K}{\sigma_0}\right)^2 \tag{13}$$

Similarly, the ratio of the CPZ at a given R-ratio, CPZ_R, over the corresponding CPZ_0 at R=0, can be estimated from Eq. (12) or (13) as:

$$\frac{CPZ_R}{CPZ_0}=\left(\frac{\Delta K_R}{\Delta K_0}\right)^2 \tag{14}$$

Equations (11) and (14) seems to be generic and independent of plane stress or plane strain conditions. Figure 3a depicts the dependence of (MPZ_R/MPZ_0) and (CPZ_R/CPZ_0) at threshold as a function of applied R-ratio for 7475-T7351 for both LT and TL orientations from R=constant and K_{max} = constant tests [22,23]. It is seen from Fig. 3a that for R < (0.6-0.7) there is a modest increase in (MPZ_R/MPZ_0) ratio from 1 to around 3, and for R > 0.7 this ratio increases exponentially up to more than 100. A similar behavior of the monotonic and cyclic plastic zone ratios for Ti-6AL-4V alloy [24] corresponding to two FCG rates $1x10^{-9}$ and $1x10^{-10}$ m/cycle is depicted in Fig. 3b. In both figures the decrease in the CPZ ratios (CPZ_R/CPZ_0) is from 1 to around 0.12-0.2 and is relatively small in comparison to exponential changes of the MPZ ratios.

4.0 A Damaging SIF Function K_d for FCG Analyses

For a cracked specimen subjected to cyclic loading at $R \geq 0$, the SIF amplitude $K_a = (K_{max}-K_{min})/2$. Adopting the stress-based function Eq. (8) in terms of K_{max} and K_a, the proposed damaging SIF function K_d for FCG analysis is given as.

$$K_d = \sqrt{K_{max} K_a} \quad \text{valid for } R \geq 0 \tag{15}$$

In the above equation K_{max} and K_a are surrogates for the intensity of the local stresses σ_{max} and σ_a in the CPZ. The product of $K_{max} K_a$ represents the intensity of the total elastic strain and complementary energy near the crack tip. The local values of σ_{max} and σ_a within the CPZ can be calculated using finite element analysis (FEA) or by an approximate method such as Neuber's rule [25]. As illustrated in Fig. 2, the local value of the R_σ within the CPZ depends on the actual location of the material point within the CPZ. On the other hand, Eq. (9) given in terms of K_{max} and K_a is independent on the localization of the material point within the CPZ. Equation (15) can be used, as a first approximation, for cyclic loading with moderate R < 0 by assuming, $K_a = K_{max}/2$.

It can be noted that Eq. (15) is subjected to some limitation regarding its associations with the total elastic damaging stress intensity K_d instead of the local elastic-plastic stresses and strains. This limitation can be resolved by calculating or estimating the local elastic-plastic σ_{max} and ε_a within the CPZ.

It can be note, that K_d value given by Eq. (15) reduces to da/dN - ΔK curve at R = 0.5. In other words, Eq. (15) converts any R-ratio data into a "master" curve corresponding to da/dN curve at R=0.5. This is in contrast to ΔK_{eff} approach, which aims to collapse the da/dN data for any R-ratio into closure free da/dN curve usually for R>0.7. It is often assumed that for R > 0.7 there is no crack closure, yet the R-ratio dependence for R > 0.7 is observed. Such dependence for R>0.7 is frequently inferred to other mechanisms of closure as roughness induced crack closure (RICC) or corrosion induced crack closure (CICC) [7, 8]. An exponential increase in the size of the MPZ_R as it shown in Figs. 3 and 4 could contribute significantly to upsurge of plasticity dissipation in the MPZ for $R > 0.7$. Therefore, such surge in energy dissipation for R > 0.7 would

reduce an apparent K_d given by Eq. (9). This increase in dissipation for R > 0.7 is overlooked in the ΔK_{eff} approach. In the author's opinion, this could contribute to unresolved challenges when ΔK_{eff} is utilized in FCG analysis. In addition, a "master" closure free da/dN vs. ΔK_{eff} curve corresponding to a high R=0.7-0.9 may induce a different failure mode in comparison to low R-ratio tests [26].

5.0 Analyses of R-ratio Effects

A threshold and FCG data used in this study are collected from the open literature with R-ratios varied from 0.1 to 0.96. All the threshold data are taken at near threshold crack growth region of ~10^{-10} m/cycle. A wide range of materials chosen for this study include steels, Al, Ti alloys and copper.

5.1 Effects of R-ratio on K_D at the threshold region

Figures 4a and 4b depict the damaging SIF function at threshold region $K_{d,th}$ versus R-ratio for 7475-T7351 [22,23] and Ti-6Al-4V [24] alloys, respectively. In both figures the dependence of $K_{d,th}$ versus R is similar despite different mechanical properties of these alloys, different testing conditions, R=constant or K_{max}=constant and even different crack growth rates of $1x10^{-9}$ or $1x10^{-10}$ m/cycle. It seems that such dependency has a general form. An examination of Figs. 4a and 4b indicates that $K_{d,th}$ is nearly constant up to R = 0.6-0.7. For larger R than 0.6 -0.7 it increases sharply and some correction is needed, which will be discussion in Section 6.

Figure 5 shows the correlation of $K_{d,th}$ versus R-ratios at threshold for EPT (Electrolytic Tough Pitch) copper with 99.95% purity in three conditions; annealed ($\sigma_{0.2}$ = 67 MPa), quarter-hard ($\sigma_{0.2}$ = 188 MPa), and full-hard ($\sigma_{0.2}$ = 194 MPa) [27]. Interestingly, these three materials have nearly the same ultimate tensile strengths of 263, 246 and 249 MPa, respectively. FCG tests were conducted in air at R-ratios of 0.1, 0.3, 0.5, and 0.7. All the specimens were precracked in accordance with ASTM Standard E647.

Annealed samples show a considerable amount of cyclic hardening whereas quarter-hard and full-hard show cyclic softening. Even though annealed, quarter-hard, and full-hard materials

have significantly different monotonic yield strengths, they have approximately the same order of cyclic yield strengths of 134, 162 and 177 MPa, respectively. This seems to be consistent for a material with high stacking fault energy by possessing a similar cyclic stress-strain curve. Annealed and quarter-hard materials show similar behavior of $K_{d,th}$ with R-ratio. On the other hand, the full-hard copper have much lower $K_{d,th}$ values. Some small drop in $K_{d,th}$ with increasing R, for annealed material, could be associated with reported reduction in oxide thickness layer formation with increasing R [27].

5.2 Correlation of R-ratio effects on FCG using K_d function

The proposed damaging stress intensity function K_d, given by Eq. (15), is utilized to correlate R ratio effects on FCG behavior for wide range of R-ratios ranging from - 2 to 0.9. Figures 6a – 9a show da/dN data versus applied ΔK for AISI 4340 steel [28], 7075-T7351 (LT) Al [22,23], 7075-T6 Al [29] and 2024-T3 Al [29]. Figures 6b – 9b depict the corresponding da/dN versus K_d. The effect of R-ratio on FCG in pure copper at three heat conditions in terms of applied ΔK is shown in Fig. 10a-c [27] and proposed K_d function in Fig. 10d.

It can be noted that Eq. (15) was utilized with no fitting or adjustable parameter when calculating K_d and all the FCG data presented in in Figs. 6– 10 form a relatively narrow scatter band in terms of K_d except R=0.9 in Fig. 8b. The effects of high R-ratio and large MPZ and associated plastic dissipation and its effects on FCG correlations is discussed in the following section.

6.0 Discussion

As it was mentioned previously in Section 3, the ratio of normalized monotonic plastic zone (MPZ_R/MPZ_0) increases exponentially for R>0.6.

Figures 11 a and 11b show a schematic illustration how ΔK and K_{max} constant tests effect the mutual relation between MPZ and CPZ. In general, a test conducted at K_{max}= constant would exhibit much larger ratio of MPZ/CPZ than R=constant test. This is predominately evident at threshold region. To illuminate this further, Fig.11c depicts a schematic illustration between

MPZ and CPZ at threshold for a low and high R-ratio test. It is apparent that in K_{max}=constant or high R-ratio tests, a reference material point located on the crack propagation path, would accumulate much higher monotonic plastic strain, in comparison to a low R-ratio test as the material reference point moves through the MPZ towards CPZ. As a result, during advancement of the crack tip more plastic energy would be dissipated if the MPZ is larger. And also, when a reference material point arrives into CPZ it would have higher monotonic prestrain which may affect a failure mode [e.g. 7, 26, 28]. Comprehensive threshold data for 7574-T7351 Al in TL and LT orientations obtained at R and K_{max} constant test [22,23] are shown in Fig. 12 in terms of a normalized $K_d/K_{d,R=0.5}$ ratio. An examination of Fig. 12 indicates that the $K_d/K_{d,R=0.5}$ is relatively independent of R-ratio till about R=0.6 -0.7. A fit of all Al data for R>0.7 results the following relation:

$$\frac{K_d}{K_{d,R=0.5}} = 0.57\left(\frac{1}{1-R}\right)^{0.455} \quad \text{Al for } R \geq 0.7 \tag{16}$$

It is interesting to mention that Ti alloy [24] at two FCG rate of 10^{-10} or 10^{-9} m/cycle and copper [27] (included in Fig. 12) follow the general trend of Al data. An inverse of Eq. (16) can be considered as a correction factor, β, for Al alloys for R>0.7 as:

$$\beta = \frac{1}{0.57}\left(\frac{1}{1-R}\right)^{-0.455} \quad \text{Al for } R \geq 0.7 \tag{17}$$

and

$$K_{d\,corr} = \beta K_d \tag{18}$$

Figure 13 shows the correlation of R-ratio on crack growth rates of 7075-T7351 (TL) Al alloy (from Fig. 7a) [22, 23] in terms of the proposed K_d function corrected for R= 0.8 and 0.9. using Eqs. (17) and (18). A very tide correlation is seen at the threshold region except data for R=0.1, which somewhat higher values may be related to ASTM load reduction procedure [4, 9, 30].

Figure 14 depicts comprehensive threshold data of Ti-6Al-4V alloy [24] in terms of $K_d/K_{d,\ R=0.5}$ ratio for R>0.5 together with the fitting curve of the form:

$$\frac{K_d}{K_{d,R=0.5}} = 0.763\left(\frac{1}{1-R}\right)^{0.367} \quad \text{Ti for } R \geq 0.52 \tag{19}$$

The corresponding corrector factor β for Ti-6Al-4V alloy is:

$$\beta = \frac{1}{0.763}\left(\frac{1}{1-R}\right)^{-0.367} \quad \text{Ti for } R \geq 0.52 \tag{20}$$

Figure 15 shows the effects of R- ratios and different width of C(T) specimens on FCG behavior of Ti-6AL-4V alloy [30] in terms of applied ΔK, Fig. 15a, and proposed K_d function, Fig. 15b.

Data at R=0.7 has been corrected using β given by Eq. (20). Interestingly, now all data for different R-ratios and specimens' widths are grouped into a narrow scatter band.

Authors in Ref. [24] reported FCG data obtained at several K_{max}= constant tests as it is shown in Fig. 16a and correlated with K_d function in Fig. 16b.

The proposed correction factors β for R>0.5 given in Eqs. (19) and (20) were obtained using threshold data. At the Paris region the correction factor β may be reduced due to large plastic strain amplitude which would promote an additional mean stress relaxation in the "process zone". This aspect of the proposed K_d function will require further research.

It should be noted that this formulation of the K_d function is limited to constant amplitude data. An extension of the proposed K_d function to overload and variable amplitude loading would require determination of σ_{max} and ε_a (or σ_a) in the "process zone". Then, da/dN – K_d curve corresponding to R = 0.5 shall be used as a "master " or "reference" curve within the "process zone" to determine the FCG rate utilizing cycle-by-cycle approach.

Conclusions

Based on the presented analyses the following conclusion can be drawn. Key practical implication of the proposed stress intensity function K_d is its ability to account for R-ratio effects in threshold and the Paris region of FCG. The proposed analysis eliminates the observed experimental difficulties and interpretations related to the crack closure assumption. This K_d function correlates R-ratio effects for both K_{max} and R constant tests. For R < 0.5-0.6 it doesn't

involve any fitting parameter and the observed trend is independent of material, specimen geometry, and methods of testing etc. For a high R>0.7 it utilizes an experimentally determine correction factor, which accounts for excessive plastic dissipation in the monotonic plastic zone (MPZ).

Conflict of Interest

The author attest that there is no a conflict of interest related to this manuscript.

References:

1. Paris P and Erdogan F. A Critical Analysis of Crack Propagation Laws. Journal of Basic Engineering 1963;85(4):528-534.
2. Elber W. The Significance of Fatigue Crack Closure. Damage Tolerance in Aircraft Structures, ASTM STP 486; 1971, 230-42.
3. Riddell WT, Piascik RS, Sutton MA, Zhao W, McNeill SR and Helm JD. Determining Fatigue Crack Opening Loads from Near-Crack-Tip Displacement Measurements. *Advances in fatigue Crack Closure Measurement and Analysis:* Second Volume, ASTM STP1343, R.C. McClung and J.C. Newman, Jr., Eds., American Society for Testing and materials, West Conshohocken, PA; 1999:157-174.
4. Newman JC Jr., Analysis of fatigue crack growth and closure near threshold conditions. ASTM STP-1372; 2000:227–251.
5. Pippan R, Riemelmoser FO and Bichler C. Measurability of Crack Closure. *Advances in Fatigue Crack Closure Measurement and Analysis: Second Volume*, *ASTM STP 1343*, R.C. McClung and J. C. Newman, Jr., Eds., American Society for Testing and Materials, West Conshohocken, PA; 1999:41-56.
6. McClung RC and Davidson DL. Near-tip and remote characterization of plasticity-induced fatigue crack closure. *in STP 1343 Advances in Fatigue Crack Closure Measurement and Analysis*: ASTM International Second Volume (eds. McClung, R. C. & Newman, J. C.);1999:106–127.

7. Suresh S. Fatigue of Materials. Cambridge University, Press, 2nd Edition; 2001.
8. Pippan R and Hohenwater A. Fatigue crack closure: a review of the physical phenomena. Fatigue Fract Engng Mater Struc 2017;40:471-495.
9. Newman JC Jr., Vizzini AJ and Yamada Y. Final Report on: Fatigue crack growth data base and analyses for the behavior in rotocraft materials, DOT/FAA/AR-10/3; March 2010.
10. Walker K. The effect of stress ratio during crack propagation and fatigue for 2024-T3 and 7075-T6 aluminum. In: Effects of Environment and Complex loading History on Fatigue Life, ASTM STP 462. Philadelphia, PA: American Society for Testing and Materials, 1970:1–14.
11. Kujawski D. A fatigue crack driving force parameter with load ratio effects. Int J Fatigue 2001;23:S239–46
12. Dinda S, Kujawski D. Correlation and prediction of fatigue crack growth for different R-ratios using K_{max} and ΔK^{+} parameters. Engng Fract Mech, 2004;71:1779–90.
13. Huang X, Moan T. Improved modeling of the effect of R-ratio on crack growth rate. Int J Fatigue 2007;29:591–602.
14. Vasudevan AK, Sadananda K and Louat N. Two critical stress intensities for threshold fatigue crack propagation. Scripta Metallurgica et Materiala 1993; 28: 65-70.
15. Vasudevan AK, Sadananda K, Louat N. A review of crack closure, fatigue crack threshold and related phenomena. Mater. Sci. Eng., 1994;A188:1-22.
Standard test method for measurement of fatigue crack growth rates, ASTM E-647, 2005.
16. Chandran RSK, Cao F, Newman JC Jr., Fatigue crack growth in miniature specimens: the equivalence of ΔK-correlation and that based on the change in net-section strain energy density, Scr. Mater., 2016;122:18-21.
17. Chandran RKS, New approach for the correlation of fatigue crack growth in metals on the basis of the change in net-section strain energy, *Acta Mater.*, 2017; 129:439-449.
18. Tong J, Alshammrei S, Lin B, Wigger T, Marrow T. Fatigue Crack closure: A myth or a misconception? Fatigue Fract Engg Mater Struc 2019 ;42 :2747-2763.
19. Gonzales JAO, Castro JTP, Meggiolaro MA, Gonzales GLG, Freire JLF. Challenging the "ΔK_{eff} is the driving force for fatigue crack growth" hypothesis. Int J Fatigue 2020;136:105577.

20. Vasudevan AK, Kujawski D., Analyses of K_{OP} relationship to threshold $K_{max,th}$, 2021, Engineering Fracture Mechanics;254:107561.
21. Kujawski D., An interpretation and modification of the SWT function, Int. J. Fatigue *(submitted)*
22. Lang M., A model for fatigue crack growth, part I: phenomenology. Fatigue Fract Engng Mater Struct 2000;23:587–601.
23. Lang M., A model for fatigue crack growth, part II: modelling. Fatigue Fract Engng Mater Struct 2000;23:603–17.
24. Boyce BL. Ritchie RO., Effect of load ratio and maximum stress intensity on the fatigue threshold in Ti-6Al-4V, Engineering Fracture Mechanics, 2001;68:129-147.
25. Sunder R, Andronik A, Biakov A, Eremin E, Panin S and Savkin A., Combined action of crack closure and residual stress under periodic overloads: A ractographic Analysis, Int. J. Fatigue 2016; 82: 667-675.
26. Lang M, Hartman GA, Larsen JM., Investigation of an abnormality in fatigue crack growth curves - the Marci effect. Scripta Materialia 1998;38:1803-10.
27. Liaw PK, Leax TR, Williams RS, Peck MG., Near-threshold fatigue crack growth behavior in copper. Metall Trans A 1982;13:1607–18.
28. Dennis JR. Fatigue crack growth of gun tube steel under spectrum loading. MS Thesis, Engineering Science and Mechanics Dert.,Virginia Polytechnic Institute and State University, Blackburg, VA, May 1986.
29. Hudson CM., Effects of stress ratio on fatigue crack growth in 7075-T6 and 2024-T3 aluminum alloy specimens. 1969, NASA TN D-5390, National Aeronautics and Space Administration, Langley Research Center, Hampton, VA.
30. Newman JC Jr., Ruschau JJ and Hill Mr., Improved test method for very low fatigue-crack-growth-rate data. 2010, Fatigue Fract Engng Mater Struct; 34:270–279.

FIGURES

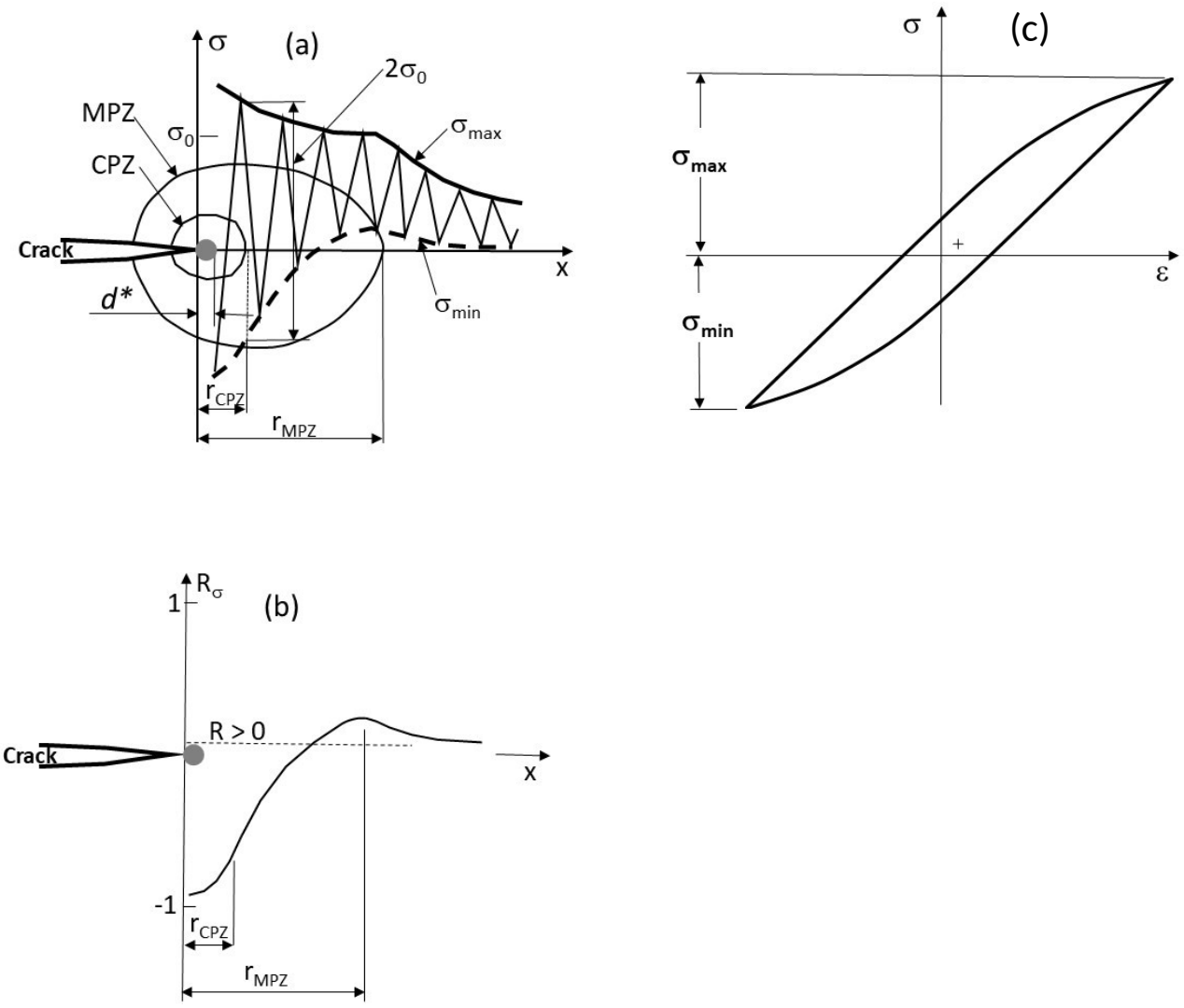

Figure 1 Schematic plot of (a) the cyclic stress distribution, (b) the stress ratio R_σ in the crack tip region, (c) the hysteresis loop within the CPZ.

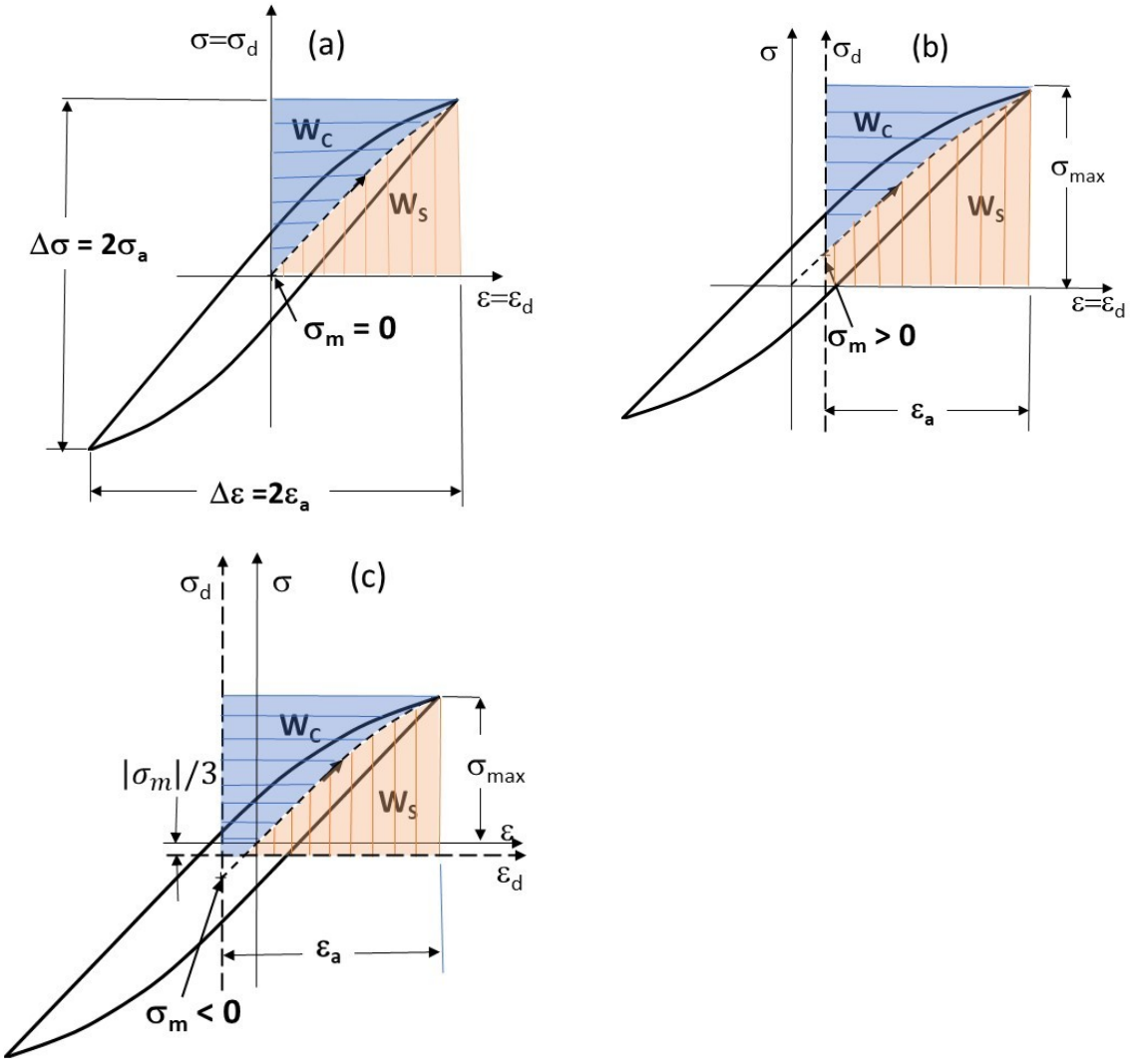

Figure 2 Schematic plot of the damaging total energy density $W_d=W_S+W_C$ and associated damaging axes σ_d–ε_d for (a) fully reversed cycling with $\sigma_m = 0$, (b) cyclic with $\sigma_m > 0$, (c) cyclic with $\sigma_m < 0$ [21].

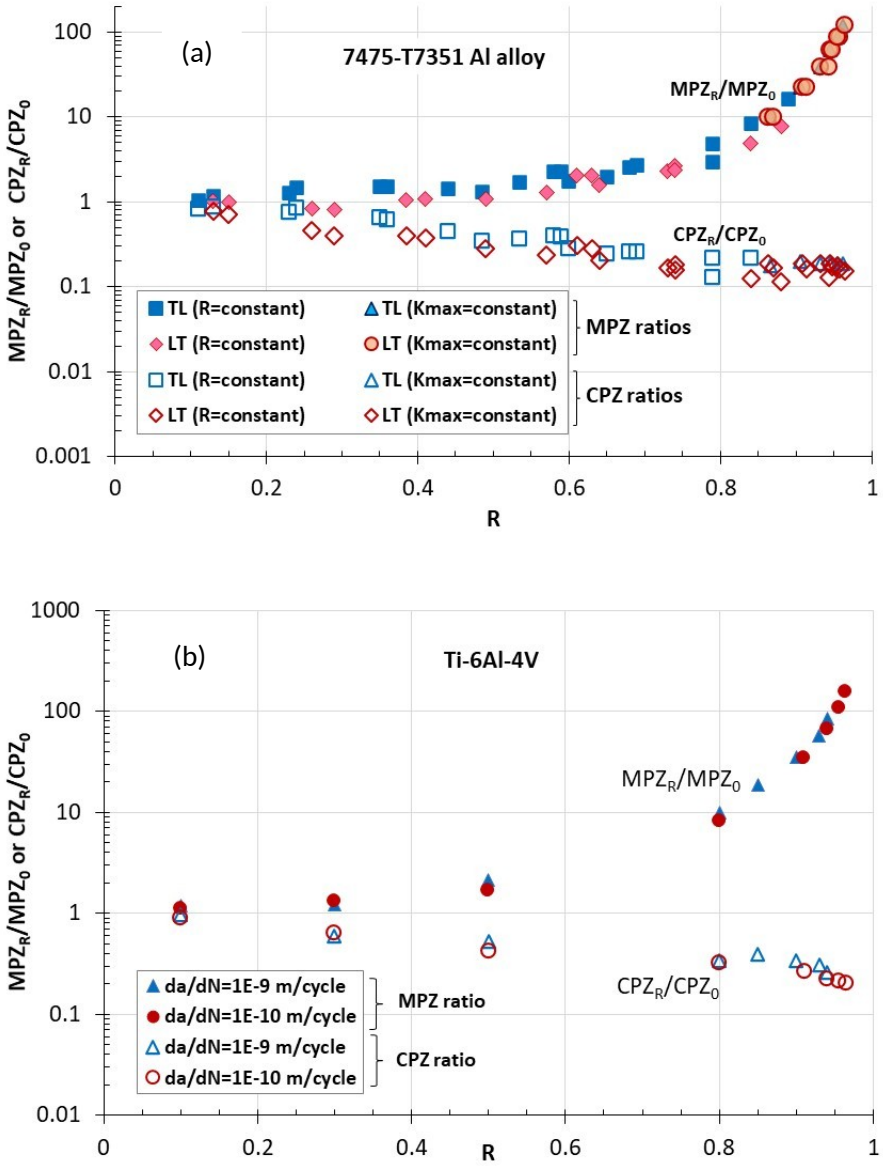

Figure 3 Normalized monotonic and cyclic plastic zone ratios in threshold for (a) Al alloy [22,23], and (b) Ti alloy at two FCG rates [24].

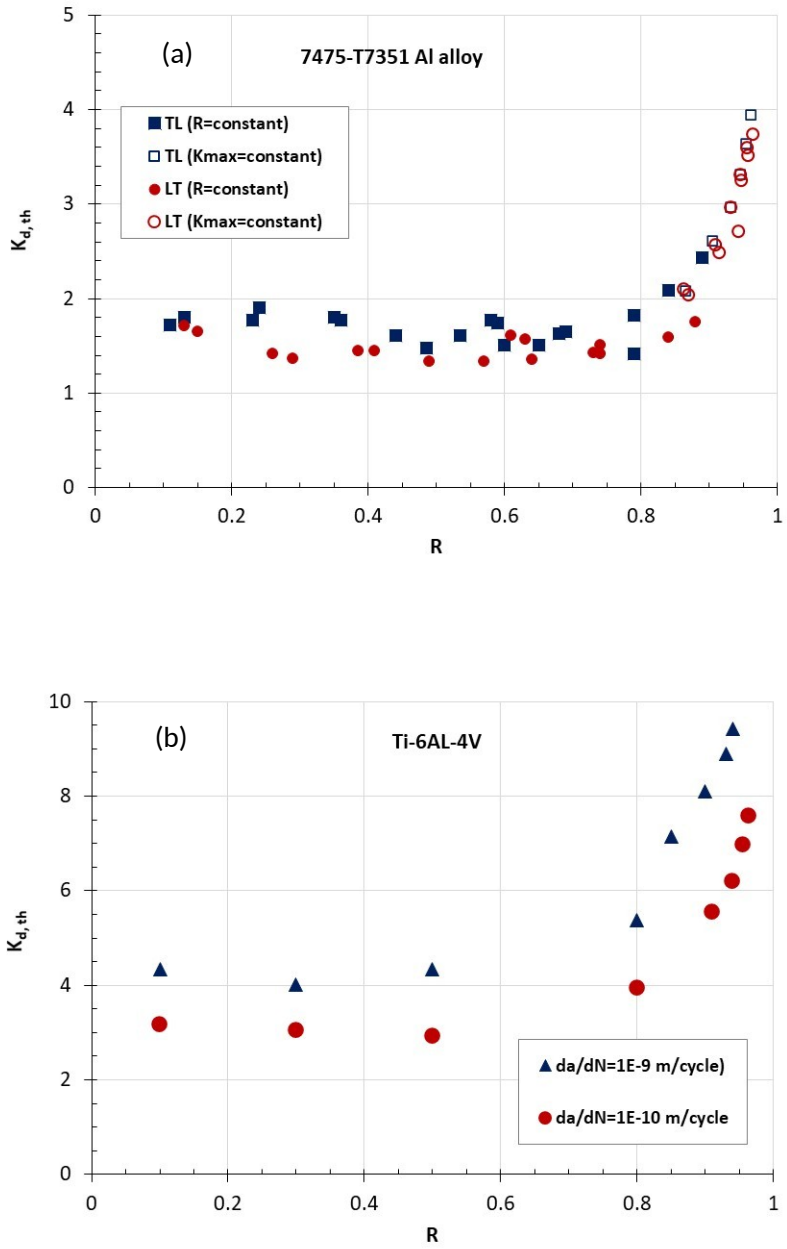

Figure 4 Effect of R-ratio on damaging stress intensity function $K_{d,\,th}$ at threshold for (a) Al alloy [22,23], and (b) Ti alloy [24].

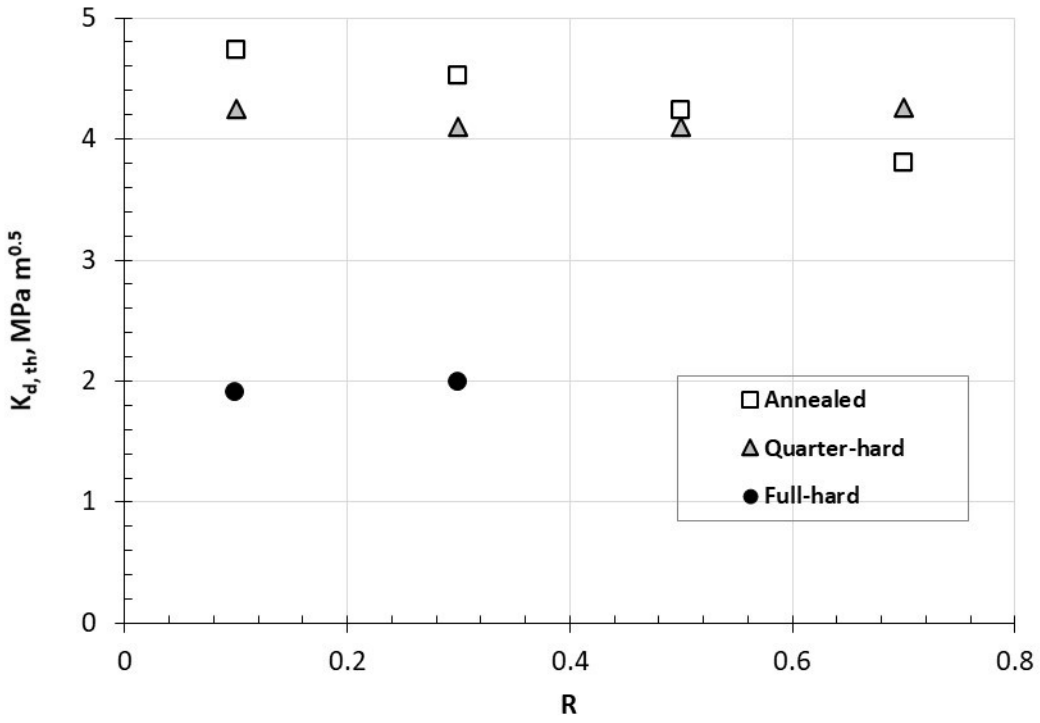

Figure 5 Effect of R-ratio on damaging stress intensity function $K_{d,\,th}$ at threshold for copper at different conditions [27]

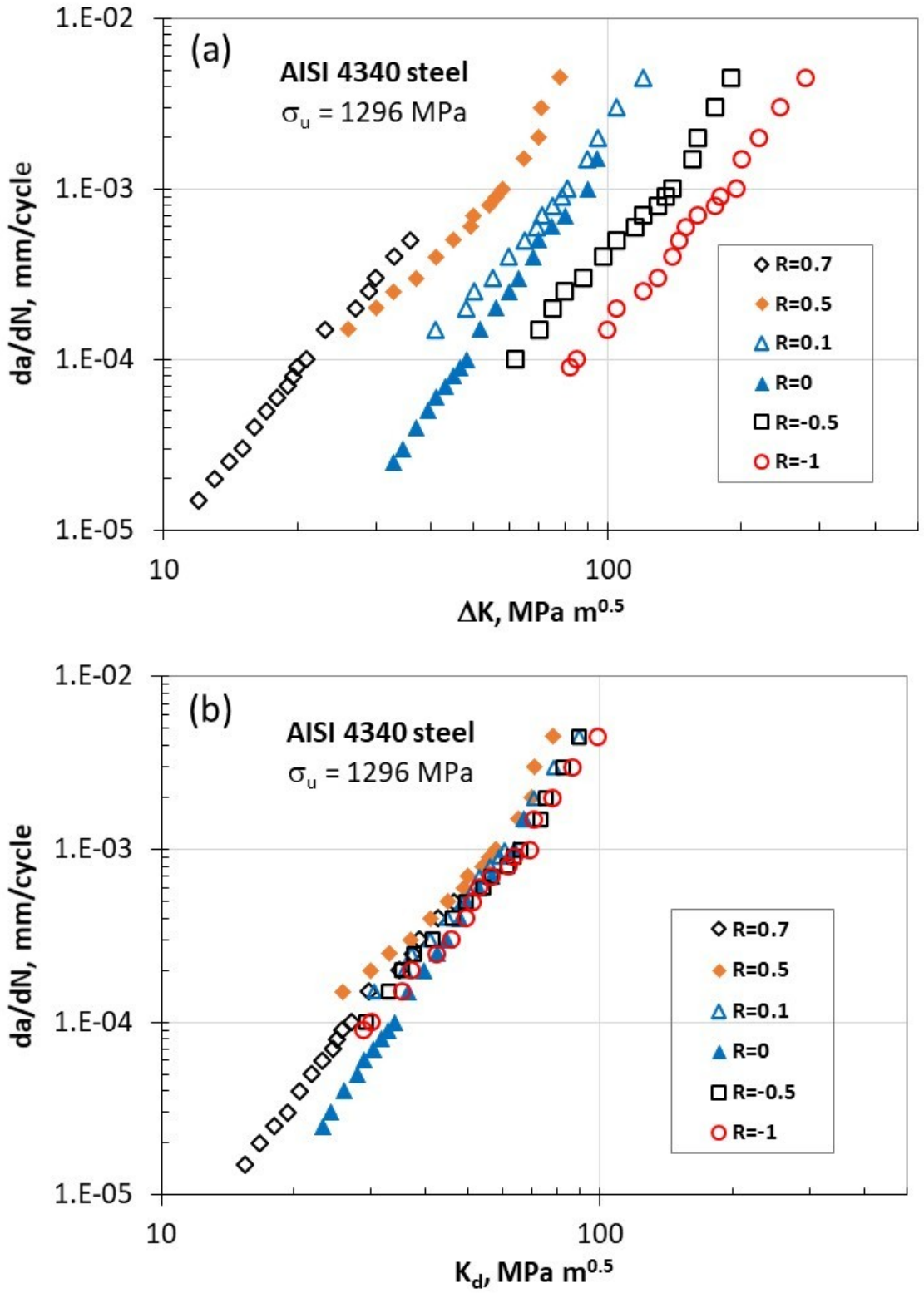

Figure 6 Effect of r-ratio on crack growth rate da/dN for an alloy steel in terms of (a) applied ΔK, and (b) proposed K_d function [28].

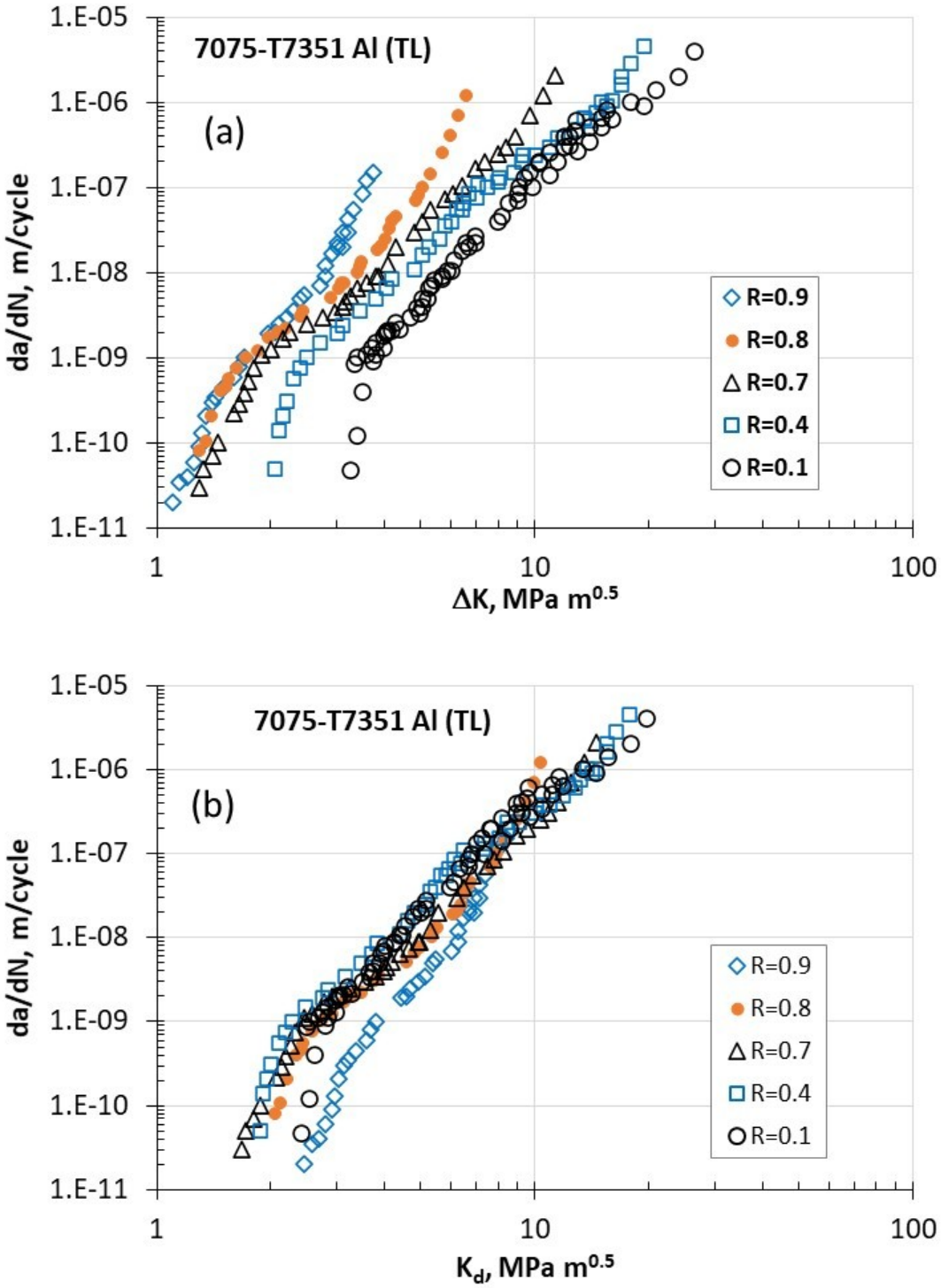

Figure 7 Effect of R-ratio on crack growth rates da/dN for an Al alloy in terms of (a) applied ΔK, and (b) proposed K_d function [22,23].

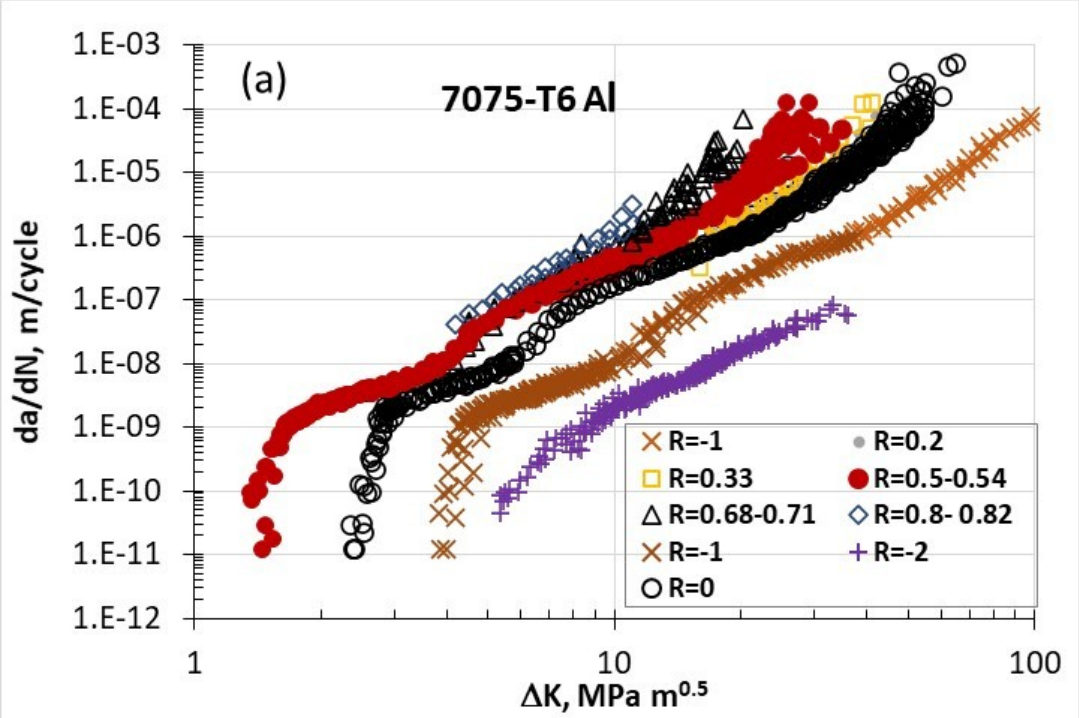

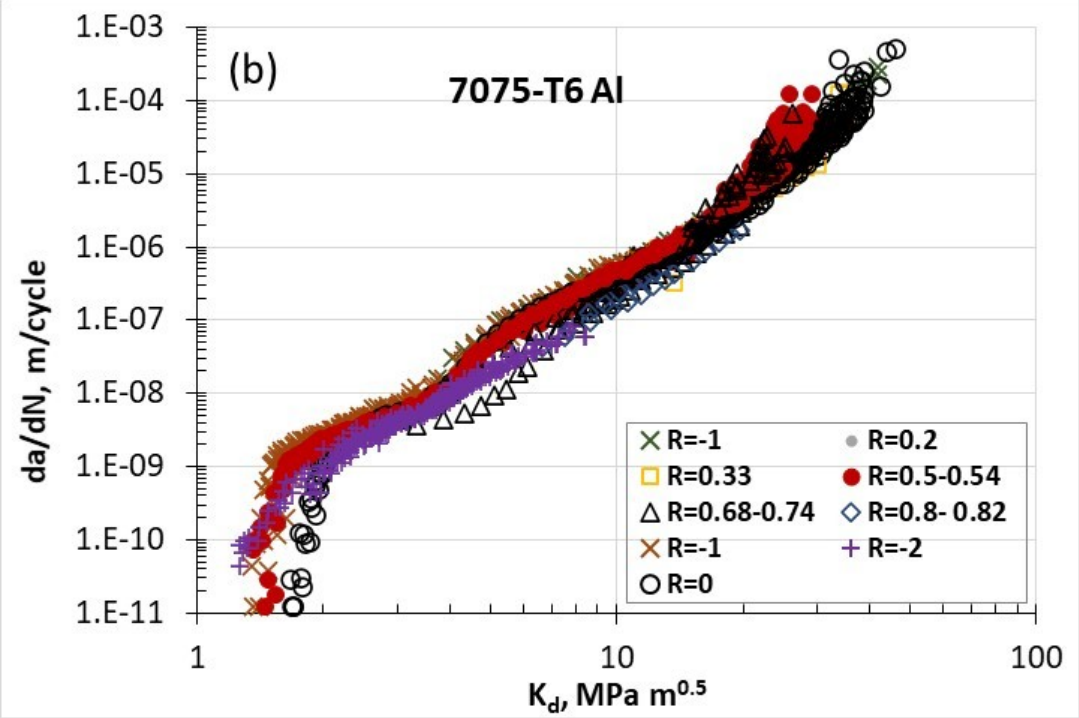

Figure 8 Effect of R-ratio on crack growth rates da/dN for an Al alloy in terms of (a) applied ΔK, and (b) proposed K_d function [29].

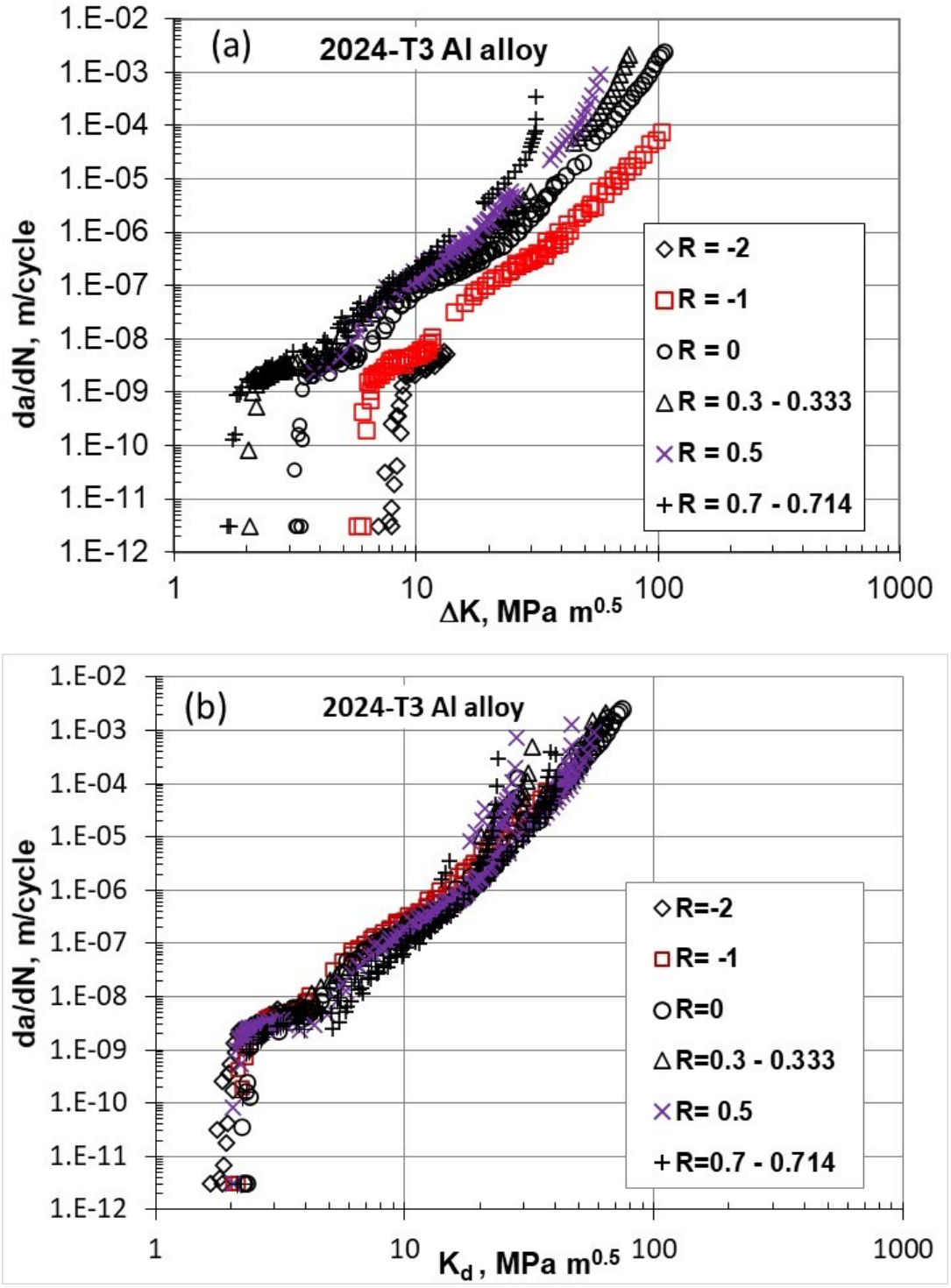

Figure 9 Effect of R-ratio on crack growth rates da/dN for an Al alloy in terms of (a) applied ΔK, and (b) proposed K_d function [29].

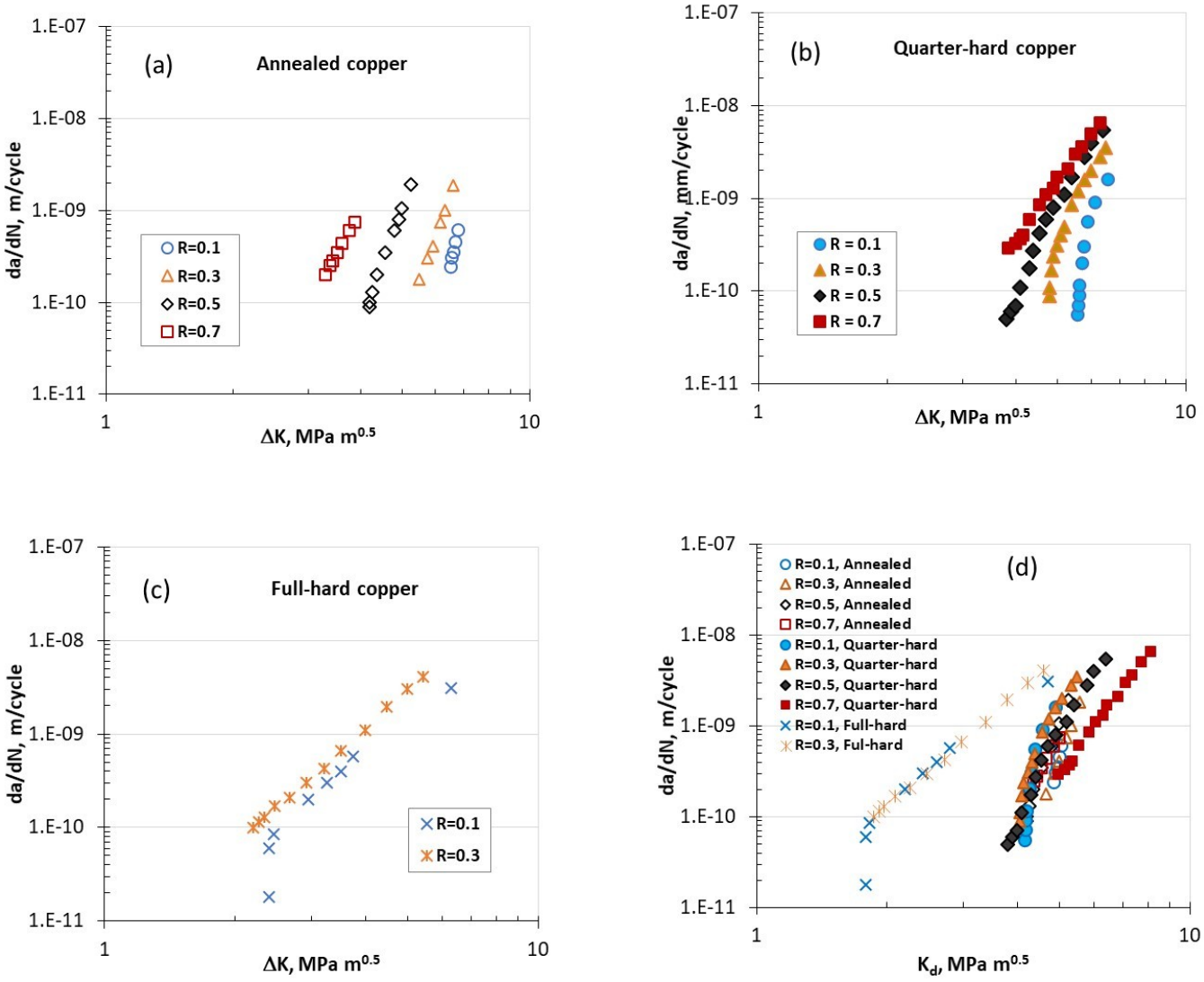

Figure 10 Effect of R-ratio on crack growth rates da/dN for pure copper at three heat conditions in terms of applied ΔK (a), (b), (c), and (d) proposed K_d function [27].

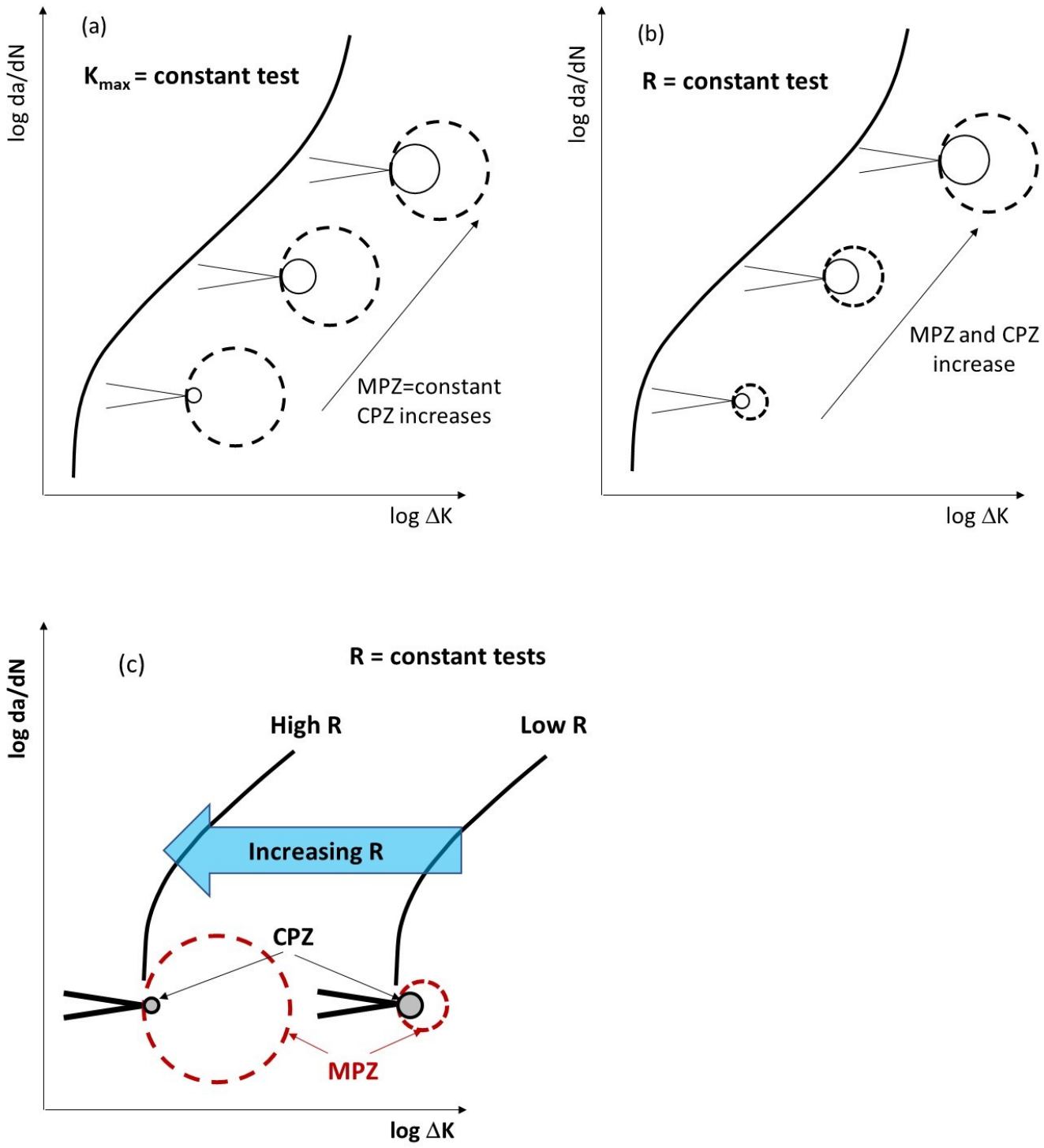

Figure 11 A schematic illustration of MPZ and CPZ for (a) constant K_{max} test, (b) constant ΔK test, and (c) for low and high R-ratio tests near the threshold.

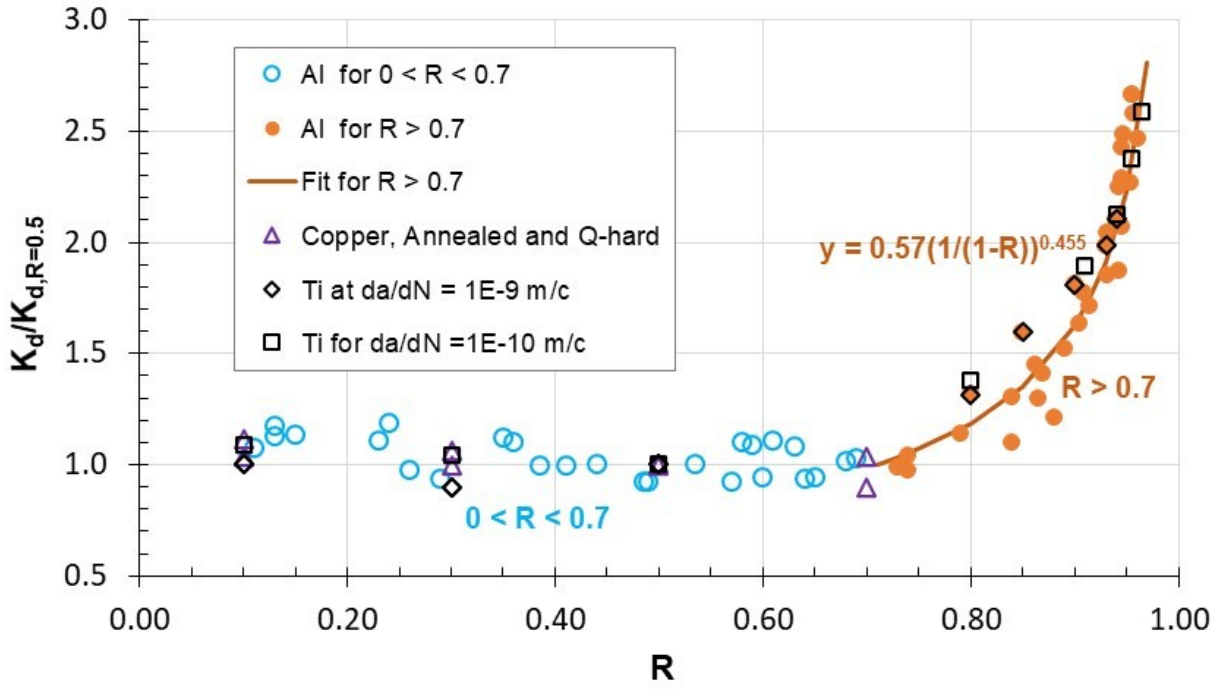

Figure 12 Effect of R-ratio on normalized $K_d/K_{d,\,R=0.5}$ at threshold for three materials investigated [22-24, 27].

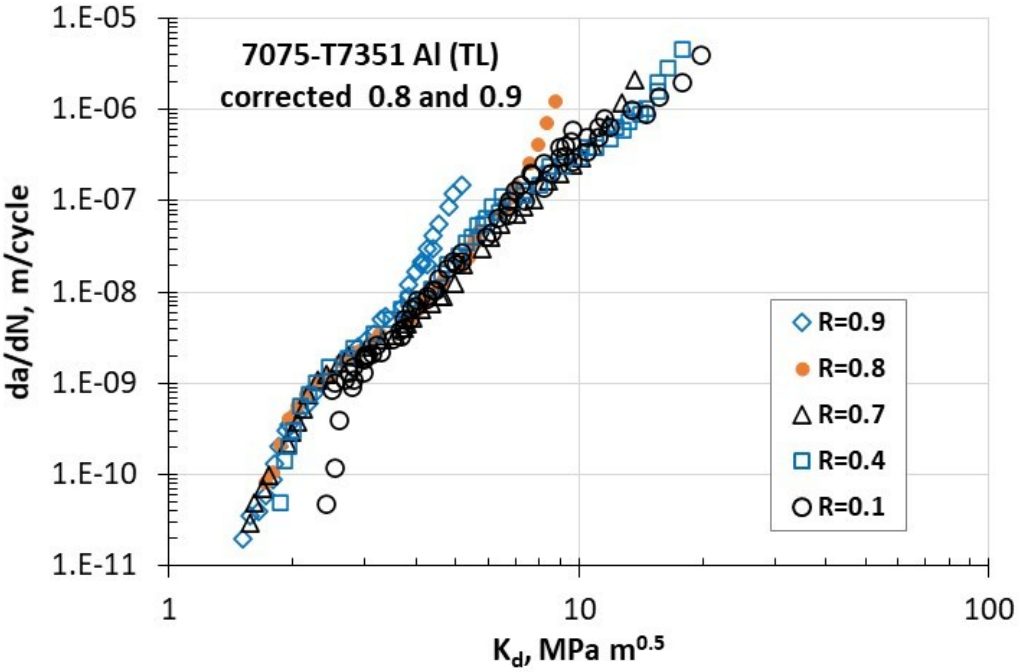

Figure 13 Effect of R-ratio on crack growth rates 7075-T7351 (TL) Al alloy (from Fig. 9a) in terms of the proposed K_d function corrected for R= 0.8 and 0.9 [22, 23].

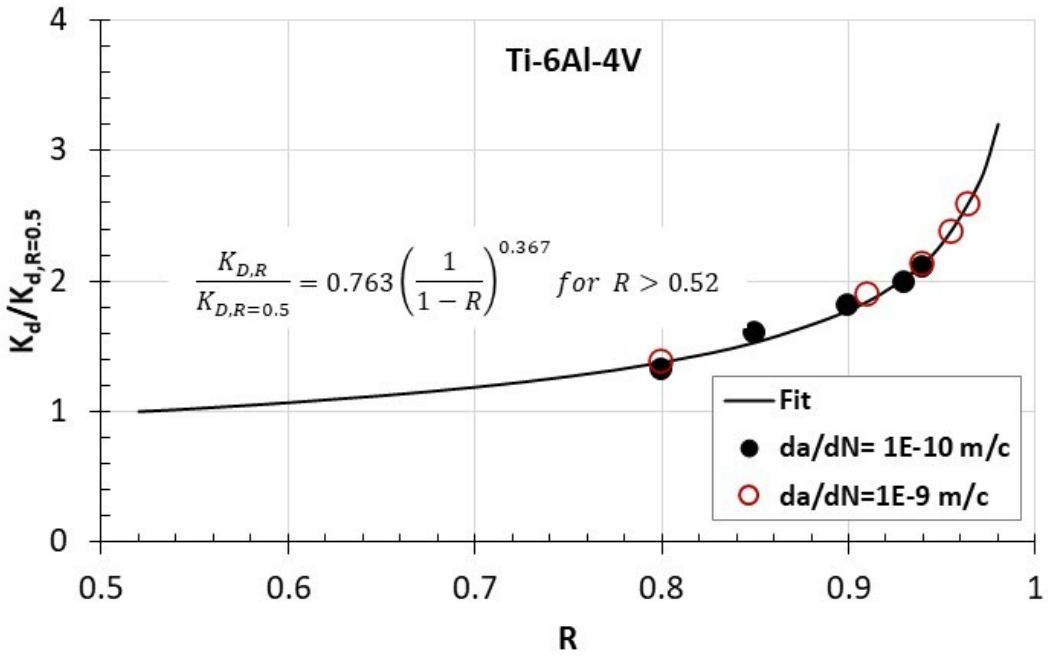

Figure 14 Effect of R-ratio on normalized $K_d/K_{d,\ R=0.5}$ at threshold of Ti-6Al-4V alloy for two FCG rates [24].

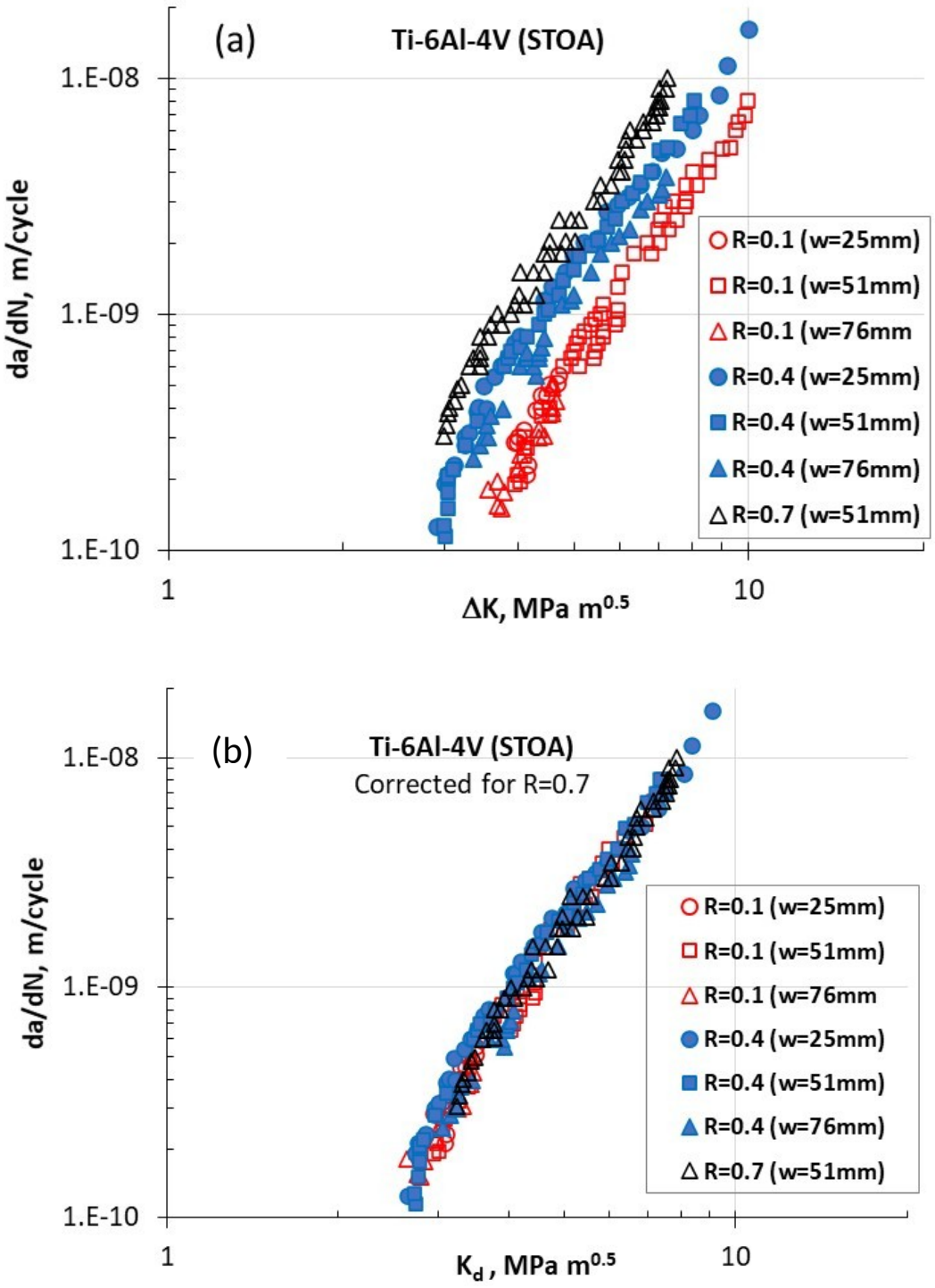

Figure 15 Effect of R-ratio and specimen width on crack growth rates da/dN for Ti alloy in terms of (a) ΔK applied, and (b) the proposed K_d function [30].

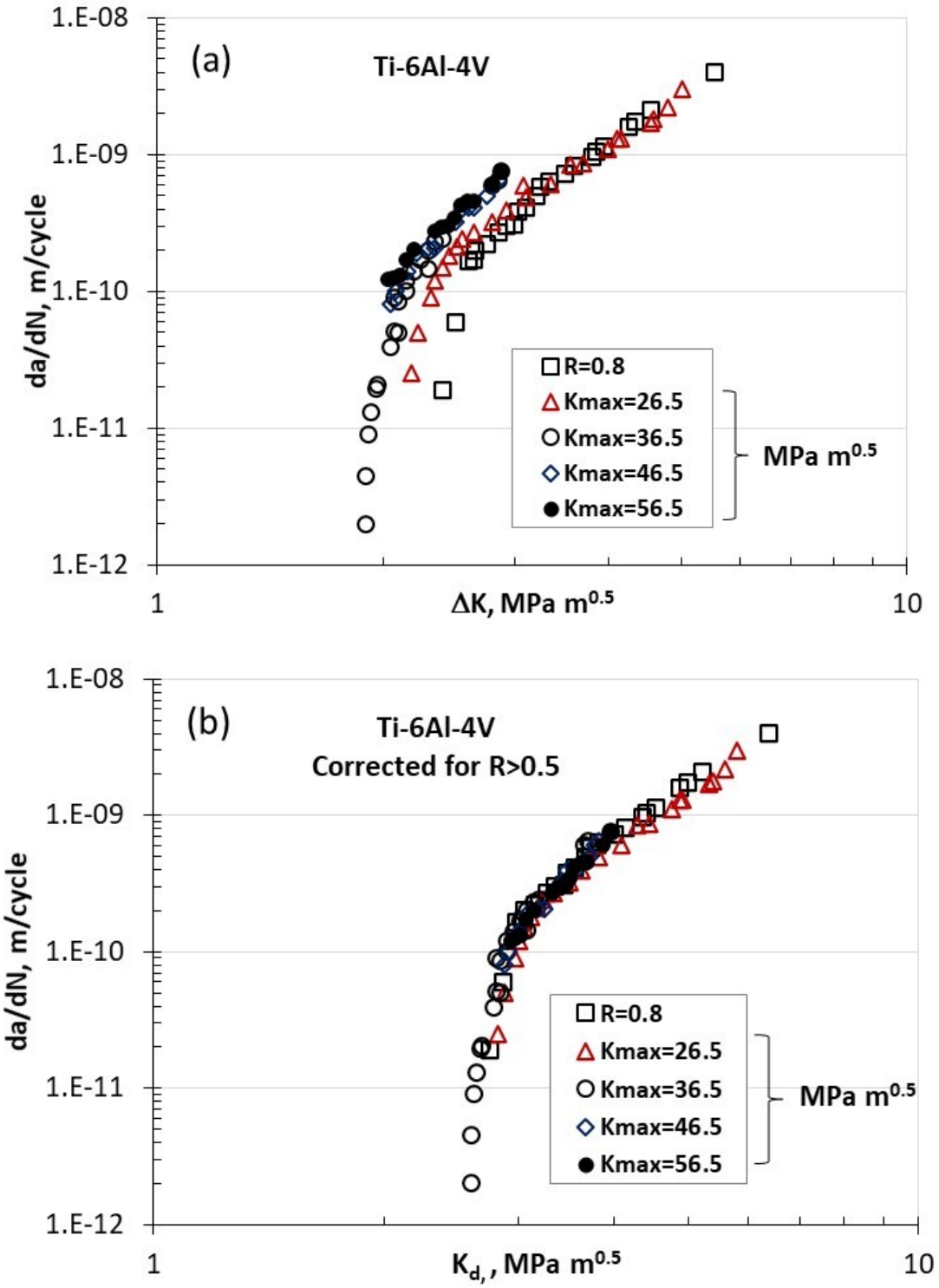

Figure 16 Effect of K_{max} on crack growth rates for Ti-6Al-4V alloy in terms of (a) applied ΔK, and (b) proposed K_d function with correction for R>0.5 [24].